Received September 26, 2020, accepted October 8, 2020, date of publication October 13, 2020, date of current version October 26, 2020.

Digital Object Identifier 10.1109/ACCESS.2020.3030719

A Karhunen-Loeve Galerkin Online Modeling Approach for the Thermal Dynamics of Li-Ion Batteries

WENJING SHEN[1], (Member, IEEE), KANGKANG XU[2], (Member, IEEE), LIMING DENG[3], AND SHUPENG ZHANG[4], (Member, IEEE)

[1]Sino-German College of Intelligent Manufacturing, Shenzhen Technology University, Shenzhen 518118, China
[2]School of Electro-Mechanical Engineering, Guangdong University of Technology, Guangzhou 510006, China
[3]Ping An Technology at Shenzhen, Shenzhen 518118, China
[4]College of Urban Transportation and Logistics, Shenzhen Technology University, Shenzhen 518118, China

Corresponding author: Shupeng Zhang (zhangshupeng@sztu.edu.cn)

This work was supported in part by the National Natural Science Foundation of China under Grant 51906160, in part by the Natural Science Foundation of Guangdong Province under Grant 2018A030313747, and in part by the Natural Science Foundation of Top Talent of SZTU under Grant 1814309011180003.

ABSTRACT The thermal dynamics of Li-ion batteries are very complicated, and the battery temperature is spatially distributed imbalanced from the battery interior to the surface. The thermal dynamics are commonly modeled by partial differential equations (PDEs); however, parameter identification for PDEs is difficult and time consuming. In this work, a Karhunen-Loeve Galerkin method is proposed to obtain a simple but effective low-order model for the distributed thermal dynamics of Li-ion batteries. The Karhunen-Loeve decomposition method is applied to capture the most representative spatial modes of the dynamics, while the Galerkin method is used to obtain the corresponding temporal modes. All the uncertain physical parameters in the temporal modes are identified by the Levenberg-Marquardt algorithm. The updated temporal modes synthesized with spatial modes can offer a fast estimation of the temperature distribution on the battery surface and thus has the potential to provide distributed temperature prediction for the battery management system. The proposed modeling scheme is tested on a 60Ah Li-ion battery cell, and the simulation result shows an excellent match in the temperature distribution and a faster computing speed than the rigorous physical model.

INDEX TERMS Li-ion batteries, Karhunen-Loeve Galerkin method, spatiotemporal separation, temperature distribution, parameter identification.

NOMENCLATURE

$\boldsymbol{A}$	matrix of partial derivatives of the terminal voltage with respect to the parameter vector, $\boldsymbol{p}$
a	specific area of the battery $[m^{-1}]$
a_p	specific area of the positive electrode $[m^{-1}]$
a_n	specific area of the negative electrode $[m^{-1}]$
C_p	volume averaged specific heat capacity at constant pressure $[Jkg^{-1}K^{-1}]$
d	thickness of the battery cell in the direction perpendicular to the parallel electrodes $[m]$
E	cell voltage $[V]$
E_{oc}	open-circuit potential of the cell $[V]$
h	convective heat-transfer coefficient on the battery surface $[Wm^{-2\circ}C^{-1}]$
J	current density $[Am^{-2}]$
k_x	effective thermal conductivities along the x direction $[wm^{-1}K^{-1}]$
k_y	effective thermal conductivities along the y direction $[wm^{-1}K^{-1}]$
n_x	number of measurements in the x direction
n_y	number of measurements in the y direction
n_t	number of measurements within the time
N	order of the low order model
$\boldsymbol{p}$	parameter vector $[p_1, p_2, p_3]^T$
p_1	representative of $k_x / \rho C_p$
p_2	representative of $k_y / \rho C_p$

The associate editor coordinating the review of this manuscript and approving it for publication was Mark Kok Yew Ng.

p_3	representative of $1/\rho C_p$
$\Delta \boldsymbol{p}$	parameter correction vector
q	heat generation rate per unit volume $[wm^{-3}]$
q_{conv}	heat dissipation rate through the battery surface by convection $[wm^{-3}]$
r_p	resistance of the positive electrode $[\Omega]$
r_n	resistance of the negative electrode $[\Omega]$
Δt	sampling interval for discretization $[s]$
T	temperature $[^\circ C]$
T_{air}	ambient temperature $[^\circ C]$
Z	x-y coordinates (x, y)

GREEK SYMBOLS

λ	algorithmic parameter value
γ_i	i-th eigenvector
λ_i	i-th eigenvalue
ζ	x-y coordinates (x, y)
ρ	density $[kgm^{-3}]$
$\theta(t)$	time variable
$\hat{\theta}(t)$	estimated time variable
$\varphi(x, y)$	spatial basis function
ϕ_p	potential distribution of the positive electrode $[Vm^{-2}]$
ϕ_n	potential distribution of the negative electrode $[Vm^{-2}]$

ACRONYMS

BMS	battery management system
BF	basis function
EV	electric vehicle
FDM	finite difference method
FEM	finite element method
HEV	hybrid electric vehicle
K-L	Karhunen-Loeve
LIB	Li-ion battery
LM	Leverberg-Marquadt
NSVM	nonlinear state variable modeling
ODE	ordinary differential equation
PDE	partial differential equation
POD	proper orthogonal decomposition

I. INTRODUCTION

The ability to monitor and control the temperature of Li-ion batteries (LIBs) is critical to avoid overheating. There are many related works on the estimation of temperature, which can be classified into two categories: lumped estimations [1]–[3] and distributed estimations [4]–[6]. In lumped estimations, equivalent-circuit models [7]–[9] are coupled with a lumped thermal model to predict the average temperature of the battery. This may lead to oversimplification in the modeling of large-scale batteries used in electric vehicles (EVs) and hybrid electric vehicles (HEVs), as significant uneven temperature distribution in space can be created depending on the driving conditions and the type of heating and cooling. Artificial neural network has also been applied to the development of empirical battery thermal models [10], [11]. On the other hand, a physics-based electrochemical model [12]–[16] coupled with distributed thermal models can improve the model's capability and capture the thermal dynamics accurately. However, these models are described in complex partial differential equations (PDEs), and cannot be used directly for online estimation and control, due to the extensive computational load and uncertain model parameters. A reliable model-reduction method and an online-parameter identification scheme are particularly desired to accurately estimate the temperature distribution in different operating conditions.

Since physics-based models are quite computationally expensive, several approximations have been made by researchers. For example, the finite difference method (FDM) [17] and finite element method (FEM) [18] are used to discretize the PDE model into an ordinary differential equation (ODE) model. These methods use local spatial basis functions (BFs) to transform the infinite dimensional model into a finite dimensional high-order temporal model, which are time consuming to compute and thus not suitable for online monitoring of the battery management system (BMS) [19]–[22]. To make it more compatible for online control, some reduced order modeling approaches have been proposed for physics-based LIB models. For example, Subramian *et al.* [23] applied polynomial approximation to electrolyte diffusion. Kumar [24] proposed a volume average field equations framework in the electrodes. Guo *et al.* [25] introduced a nonlinear state variable modeling (NSVM) algorithm, which maintains all of the nonlinear features. Cai *et al.* [26] applied the proper orthogonal decomposition (POD) method to develop a one-dimensional reduced electrochemical-thermal model. Fan *et al.* [27] used the Galerkin's projection method to reduce the order of the electrochemical model. Meng *et al.* [28] applied partial least squares regression to linearize the equivalent-circuit model. However, most of the research focused on the electrochemical model or lumped thermal model. In recent years, time/space separation-based spatiotemporal modeling methods have been successfully applied to simplify the modeling of the distributed thermal dynamics among large LIBs [29]–[32].

The simplified models need to be further validated to make accurate predictions for the electric and thermal dynamics of LIBs. The accuracy of the parameters plays a critical role in model predictions. However, some parameters cannot be measured directly through experiments [12]. Many algorithms, including the gradient method [33], the gradient-free method [34]–[38] and the Kalman filter method [4], [39] have been proposed for the parameter identification of LIBs. The Leverberg-Marquadt (LM) algorithm is a classic gradient-based nonlinear regression method. LM can adjust itself between gradient descent method and Gauss-Newton method automatically to identify the parameters efficiently. Jin *et al.* [40] applied the LM algorithm to a rigorous physics-based model that can converge quickly to the optimum. Thus,

it would be a good option to propose a simple but effective low-order model to track distributed thermal dynamics.

Based on these discussions, we propose a spatiotemporal separation modeling method with LM parameter identification to obtain an equivalent low-order thermal model for a LIB cell. First, the Karhunen-Loeve (K-L) decomposition, also known as principal component analysis (PCA), is applied to compute the most characteristic spatial modes of the dynamics. Then, the temporal modes are obta–ined by Galerkin's method. This approach can generate a lower-order and more accurate model than FEM, FDM and other spectral methods [22]. The uncertain physical parameters in the temporal modes are identified by the Levenberg-Marquardt (LM) algorithm. Then, the temporal modes are updated with the identified parameters. Finally, the temporal modes are synthesized with spatial modes and offer an accurate estimation of the temperature distribution throughout the battery's surface. The main contributions of this paper are summarized as follows:

1. The K-L Galerkin procedure is applied to nonlinear distributed thermal systems of LIBs to obtain a lower dimensional dynamic model, which can decouple the time and space ties and is available for online estimation.

2. The LM algorithm is applied to identify the decomposed model parameters to achieve satisfactory performance, which demonstrates fast convergence and thus is suitable for the online identifications.

3. Our experiments demonstrate the effectiveness of the proposed method in achieving both better prediction performance and less time consumption.

The rest of this paper is organized as follows: Section II is the problem formulation. Section III introduces the K-L decomposition-based identification process. Experimental validation is given in Section IV, and the conclusions are presented in Section V.

II. THERMAL MODEL AND PROBLEM FORMULATION

Due to the uneven electrochemical reaction inside the LIBs, the heat generation rate is unevenly distributed. The two-dimensional thermal distribution model is built by coupling the uneven voltage distribution model with the transient two-dimensional equation of heat conduction [41]. It is assumed that the thickness dimension can be neglected comparing to the width and length dimensions of the battery cell. The schematic diagram of the thermal model is shown in Figure 1.

Based on the differential energy conservation for a battery, the transient two-dimensional equation of heat conduction in the cell domain is as follows:

$$\rho C_p \frac{\partial T}{\partial t} = \frac{\partial}{\partial x}(k_x \frac{\partial T}{\partial x}) + \frac{\partial}{\partial y}(k_y \frac{\partial T}{\partial y}) + q - q_{conv}, \quad (1)$$

The detailed definition of each term of (1) is described in [42].

The thermal parameters include the thermal conductivity, the heat capacity, and the density, which vary with the temperature. To achieve an accurate temperature distribution for the BMS, it is critical to identify these parameters online.

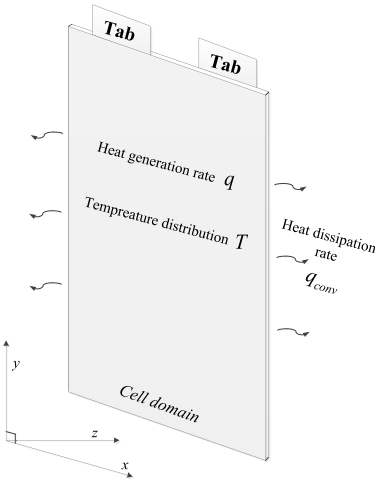

FIGURE 1. Schematic diagram of the thermal model.

To facilitate the deduction, equation (1) can be rewritten as:

$$\frac{\partial T}{\partial t} = \frac{\partial}{\partial x}(p_1 \frac{\partial T}{\partial x}) + \frac{\partial}{\partial y}(p_2 \frac{\partial T}{\partial y}) + p_3(q - q_{conv}), \quad (2)$$

The heat generation rate q is given as follows:

$$q = aJ\left[E_{oc} - E - T\frac{dE_{oc}}{dT}\right] + a_p \frac{|\nabla \phi_p|^2}{r_p} + a_n \frac{|\nabla \phi_n|^2}{r_n}, \quad (3)$$

The detailed definition of each term on the right-hand side of (3) is described in [43], [44]. The first item on the right side of (3) is the electrochemical heat generated in the porous electrode sub-domain; the second and third items are the Joule heating rates in the current collectors.

The heat dissipation rate q_{conv} is expressed as follows:

$$q_{conv} = \frac{2h}{d}(T - T_{air}), \quad (4)$$

The rate is rendered by approximating a three-dimensional object to a two-dimensional one as shown in (1). The relevant boundary conditions include the current and potential states for V_p and V_n [45].

There are two challenges associated with the thermal model identification for LIBs:

1) The model is described by PDEs with space-time coupled and high nonlinearity, making it difficult to obtain an analytical solution.
2) The computation for a numerical solution by FDM/FEM of the rigorous model is time consuming, which makes it difficult to achieve real time estimation and control application in the BMS.

Thus, it is a great challenge to propose a solution that results in time efficiency and enough accuracy to identify the parameters for the thermal model.

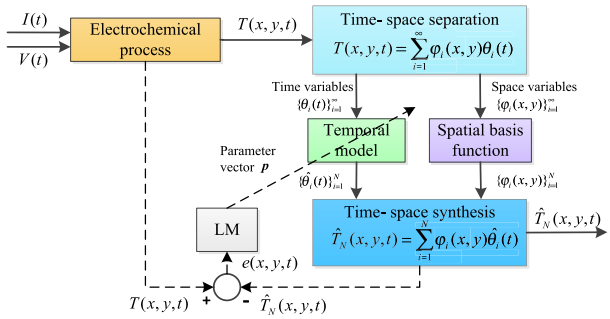

FIGURE 2. Block diagram of the K-L decomposition-based parameter identification. — represents the identification process and — represents the spatiotemporal modeling process.

III. K-L DECOMPOSITION-BASED PARAMETER IDENTIFICATION

A spatiotemporal modeling-based method is proposed to identify the parameters of the thermal model of LIBs. The block diagram of the space-time separation-based parameter identification is shown in Figure 2. This method consists of four main steps:

1) K-L decomposition is applied to obtain the spatial BFs $\{\varphi_i(x,y)\}_{i=1}^{\infty}$ of the spatiotemporal variable $T(x,y,t)$.
2) Galerkin's method is used to calculate the temporal model $\{\theta_i(t)\}_{i=1}^{\infty}$.
3) The identified physical parameters by the LM algorithm are used to adjust the temporal models.
4) The updated temporal models are synthesized with spatial BFs to estimate the temperature distribution on the battery surface.

A. TIME/SPACE SEPARATION-BASED LOW-ORDER MODELING

Motivated by the Fourier series, the spatiotemporal variable $T(x,y,t)$ can be expanded onto an infinite number of orthonormal spatial BFs $\{\varphi_i(x,y)\}_{i=1}^{\infty}$ with corresponding time variables: $\{\theta_i(t)\}_{i=1}^{\infty}$ according to the formula $T(x,y,t) = \sum_{i=1}^{\infty}\varphi_i(x,y)\theta_i(t)$. The inner product, norm and ensemble average are defined as $(f(x),g(x)) = \int_{\Omega} f(x),g(x)dx$, $\|f(x)\| = (f(x),f(x))^{1/2}$ and $\langle f(x,t)\rangle = (1/L)\sum_{t=1}^{L} f(x,t)$, respectively.

Because the spatial BFs are orthonormal, that is,

$$\left(\varphi_i(x,y),\varphi_j(x,y)\right) = \iint_{\Omega}\varphi_i(x,y)\varphi_j(x,y)dxdy = \begin{cases} 0, & i\neq j \\ 1, & i=j, \end{cases} \tag{5}$$

the time variable can be calculated from

$$\theta_i(t) = (\varphi_i(x,y), T(x,y,t)), \quad i = 1,\ldots,\infty. \tag{6}$$

In practice, it has to be truncated to a finite dimension for approximation:

$$\hat{T}_N(x,y,t) = \sum_{i=1}^{N}\varphi_i(x,y)\hat{\theta}_i(t), \tag{7}$$

where $\hat{\theta}_i(t)$ is the estimated time variable by the LM algorithm, which is discussed in Section 3.4.

B. K-L DECOMPOSITION

To obtain the spatial basis function, K-L decomposition is applied to compute the most characteristic spatial functions $\{\varphi_i(x,y)\}_{i=1}^{N}$. The spatiotemporal observations of temperature $\{T(x_m,y_l,t_k)|x_m,y_l \in \Omega, m = 1,\ldots,n_x, l = 1,\ldots,n_y, k = 1,\ldots,n_t\}$ are usually called snapshots. The observations are uniformly sampled from measurements in space-time dimensions.

The typical $\{\varphi_i(x,y)\}_{i=1}^{N}$ can be mathematically derived by optimizing the following objective function:

$$\min_{\varphi_i(x,y)} \left\langle \left\| T(x,y,t) - \hat{T}_N(x,y,t) \right\| \right\rangle, \tag{8}$$

subject to $(\varphi_i,\varphi_i) = 1, \varphi_i \in L^2(\Omega), i = 1,\ldots,N$. The orthogonal constraint $(\varphi_i,\varphi_i) = 1$ is imposed to ensure that the function $\varphi_i(x,y)$ is unique. The solution of (8) can be obtained through the following eigenvalue problem:

$$\int_{\Omega} R(Z,\zeta)\varphi_i(\zeta)d\zeta = \lambda_i\varphi_i(Z), \tag{9}$$

where $R(Z,\zeta) = \langle T(Z,t)T(\zeta,t)\rangle$ is the spatial two-point correlation function. By the method of snapshots, $\varphi_i(Z)$ can be expressed as a linear combination of the snapshots as follows:

$$\varphi_i(Z) = \sum_{t=1}^{n_t}\gamma_{it}T(Z,t). \tag{10}$$

Substituting (10) into (9) gives the following eigenvalue problem:

$$\int_{\Omega}\frac{1}{n_t}\sum_{t=1}^{n_t}T(Z,t)T(\zeta,t)\sum_{k=1}^{n_t}\gamma_{ik}T(\zeta,k)d\zeta = \lambda_i\sum_{t=1}^{n_t}\gamma_{it}T(Z,t). \tag{11}$$

The temporal two-point correlation function is defined as

$$C_{tk} = \frac{1}{n_t}\int_{\Omega} T(\zeta,t)T(\zeta,k)d\zeta. \tag{12}$$

The eigenvalue problem (11) can be transformed to the following form of an $n_t \times n_t$ matrix eigenvalue problem:

$$C\gamma_i = \lambda_i\gamma_i, \tag{13}$$

where $\gamma_i = \left[\gamma_{i1},\ldots,\gamma_{in_t}\right]^T$ is the i-th eigenvector. The solution of the eigenvalue problem (13) yields the eigenvectors $\gamma_1,\ldots\gamma_{n_t}$, which can be used in (10) to calculate the spatial BFs $\{\varphi_i(x,y)\}_{i=1}^{N}$.

The eigenvalues obtained from (13) are $\lambda_1 > \lambda_2 > \cdots > \lambda_{n_t}$ and are applied to determine the orders of the spatial basis function. The order of the low dimensional model N can be determined using the following equation:

$$\eta = \sum_{i=1}^{N}\lambda_i \Big/ \sum_{i=1}^{n_t}\lambda_i. \tag{14}$$

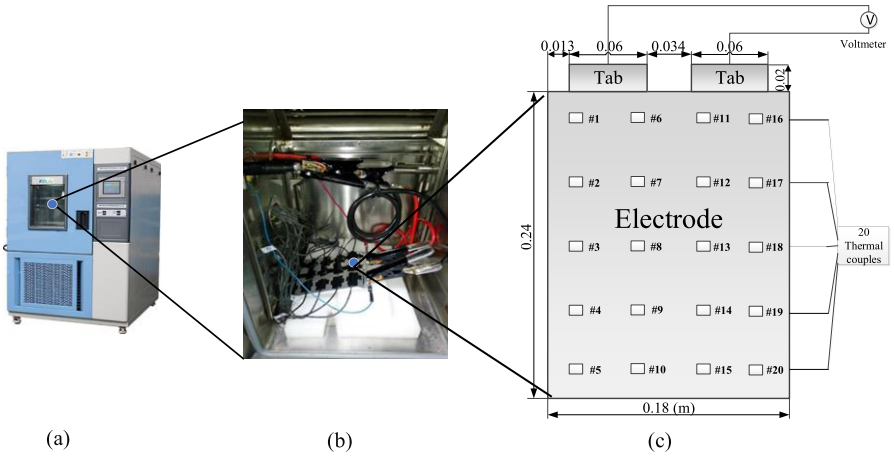

FIGURE 3. Experimental setup: (a) thermal chamber for environment temperature setting, (b) temperature measurement of the LIB, and (c) schematic plot of the locations of thermocouples.

A value of $\eta \geq 0.99$ is always taken to capture the majority characteristic [46].

C. TEMPORAL MODEL IDENTIFICATION

With the learned optimal spatial BFs $\{\varphi_i(x, y)\}_{i=1}^N$, the value of the corresponding time variables $\theta_i(t)$ can be obtained with respect to the spatiotemporal data $\{T(x_m, y_l, t_k)\}$ from (6), as follows:

$$\theta_i(t) = (\varphi_i(x, y), T(x_m, y_l, t_k)). \tag{15}$$

Substituting the truncated expansion (7) into the physics-based model (2), the equation residual can be obtained as

$$\begin{aligned}&\delta(x, y, t)\\ &= \frac{\partial T_N(x, y, t)}{\partial t}\\ &\quad - \left(p_1 \frac{\partial^2 T_N(x, y, t)}{\partial x^2} + p_2 \frac{\partial^2 T_N(x, y, t)}{\partial y^2} + p_3 (q - q_{conv})\right)\end{aligned} \tag{16}$$

and with Galerkin's method,

$$\int \delta(x, y, t)\varphi_j(x, y)d\Omega = 0. \tag{17}$$

Substituting (7) and (16) into (17) gives the following equation:

$$\int_\Omega \left(\frac{\partial \left(\sum_{i=1}^N \varphi_i(x, y)\hat{\theta}_i(t) \right)}{\partial t} - \aleph \right) \varphi_j(x, y)d\Omega = 0, \tag{18}$$

where $\aleph = p_1 \frac{\partial^2 \left(\sum_{i=1}^N \varphi_i(x,y)\hat{\theta}_i(t) \right)}{\partial x^2} + p_2 \frac{\partial^2 \left(\sum_{i=1}^N \varphi_i(x,y)\hat{\theta}_i(t) \right)}{\partial y^2} + p_3 (q - q_{conv})$

The PDEs can be reduced to a set of ODEs as follows:

$$\dot{\theta}_j(t) = \sum_{i=1}^N \psi_{ij}\theta_i(t) + \chi_j Q(t), \tag{19}$$

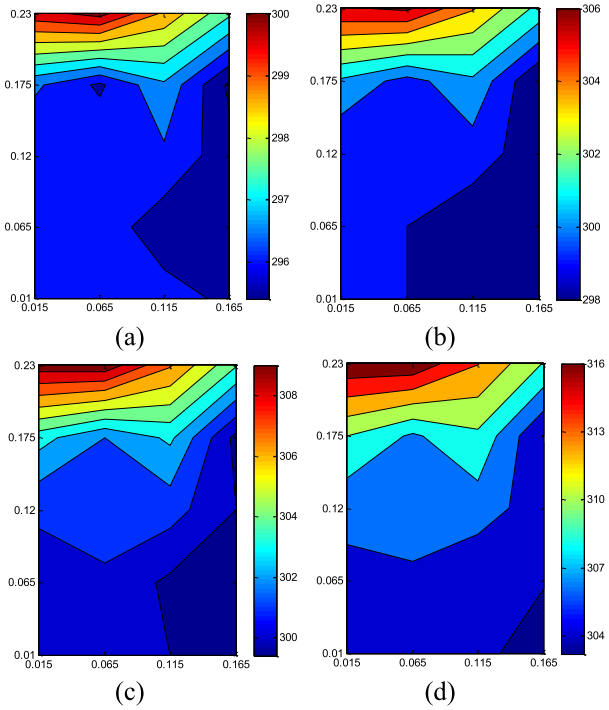

FIGURE 4. Temperature data for model identification at different times: (a) 3 min, (b) 6 min, (c) 8 min and (d) 13 min.

where $\psi_{ij} = \int_\Omega \left(p_1 \partial^2 \varphi_i / \partial x^2 + p_2 \partial^2 \varphi_i / \partial y^2\right) \varphi_j d\Omega$, $\chi_j = p_3 \int_\Omega \varphi_j dx$, $Q = q - q_{conv}$.

For practical application, a discrete form of (19) obtained by Taylor expansion is often used:

$$\theta_j(k) = \theta_j(k-1) + \sum_{i=1}^N \psi_{ij}\theta_i(k-1)\Delta t + \chi_j Q(k-1). \tag{20}$$

D. PARAMETER IDENTIFICATION

The parameters in (2) need to be identified online and the optimization procedure is as follows:

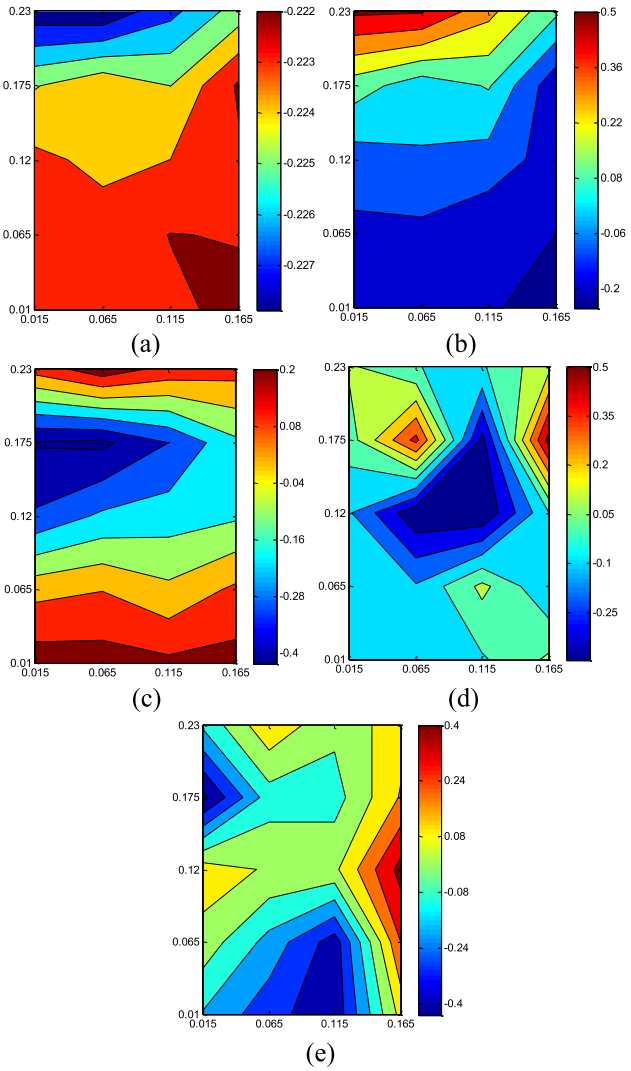

FIGURE 5. Obtained spatial basis functions for model reduction in the order of the corresponding eigenvalues: (a) first order, (b) second order, (c) third order, (d) fourth order and (e) fifth order.

1) The time variables with parameter vector $\boldsymbol{p} = [p_1, p_2, p_3]^T$ are synthesized with space functions (7) to estimate the temperature distribution $\hat{T}_N(x_m, y_l, t_k)$.

2) The objective/fitness function f is constructed for the optimal identification of the parameter vector $\boldsymbol{p}$ in the thermal model (2), which is a quadratic function of the difference between the experimental temperature $T(x_m, y_l, t_k)$ and the predicted temperature $\hat{T}_N(x_m, y_l, t_k)$:

$$f = \sum_{m=1}^{m=n_x} \sum_{l=1}^{l=n_y} \sum_{k=1}^{k=n_t} (T(x_m, y_l, t_k) - \hat{T}_N(x_m, y_l, t_k))^2 = (T - \hat{T}_N)^T (T - \hat{T}_N). \quad (21)$$

3) The LM algorithm is applied to calculate the parameter correction vector $\Delta\boldsymbol{p}$ according to the objective function in (23). The time variables are updated with the identified parameter vector $\boldsymbol{p} = \boldsymbol{p} + \Delta\boldsymbol{p}$. The procedure switches to step 1 until the objective function value is less than the preset value τ_{set}.

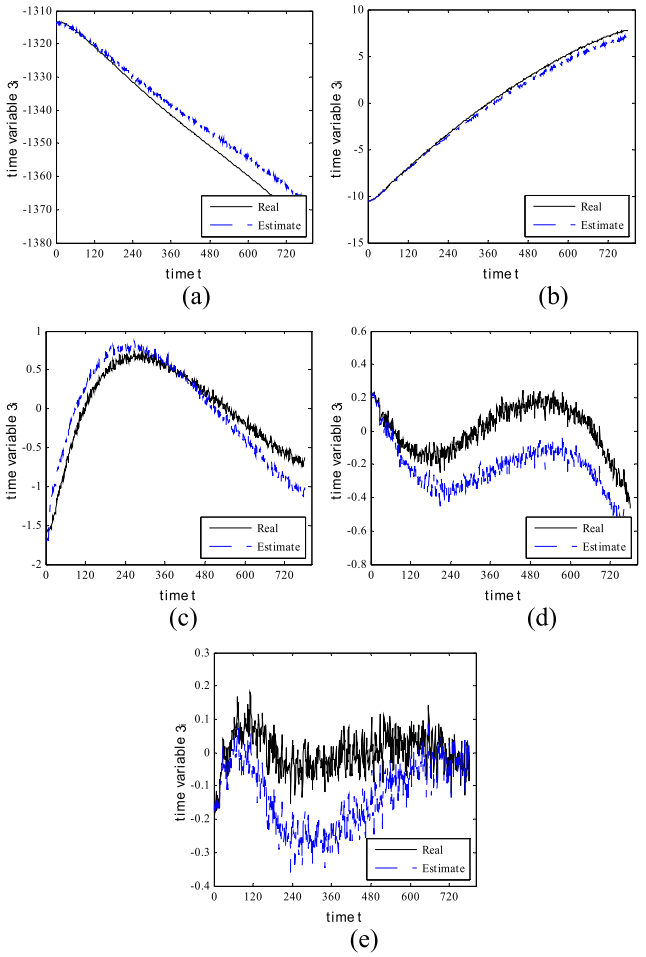

FIGURE 6. Comparison of the real and estimated time variable $\theta_j(k)$ at the (a) first order, (b) second order, (c) third order, (d) fourth order and (e) fifth order.

The parameter correction vector $\Delta\boldsymbol{p}$ is obtained based on objective function (21) and the LM method as follows:

$$\Delta\boldsymbol{p} = (\boldsymbol{A}^T\boldsymbol{A} + \lambda\boldsymbol{I})^{-1}\boldsymbol{A}^T(T - \hat{T}_N), \quad (22)$$

where $\boldsymbol{A}$ is evaluated at all the experimental temperature data. LM adaptively alters the algorithmic parameter value λ between the gradient descent one and the Gauss-Newton one. The parameter λ determines how the LM algorithm works and is initialized to be large. If the iteration results in a better approximation, then the parameter λ is decreased to 0.1λ and LM is more like a Gauss-Newton update. If the iteration provides a worse approximation, then the parameter λ is increased to 10λ and LM approaches a gradient descent update [47].

IV. EXPERIMENTAL VALIDATION

A. EXPERIMENTAL SETUP

The LIB used in this study was purchased from Shenzhen Changhe Power Technology Co., Ltd., Shenzhen, China (cell dimensions: $240 \times 180 \times 30$ mm^3), with a nominal capacity of 60Ah and a nominal voltage of 3.2 V. The active materials of the cathode and anode are $LiFePO_4$ and graphite,

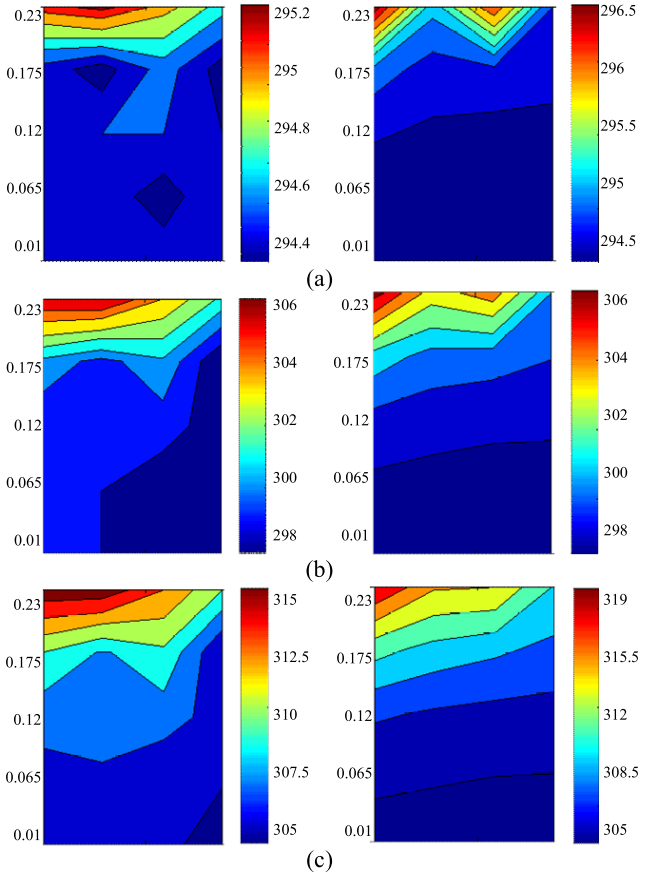

FIGURE 7. Temperature distributions based on experimental data by thermocouples (left) and modeling result by the identified parameters (right) at discharge times of (a) 1 min, (b) 6 min and (c) 13 min at 3C.

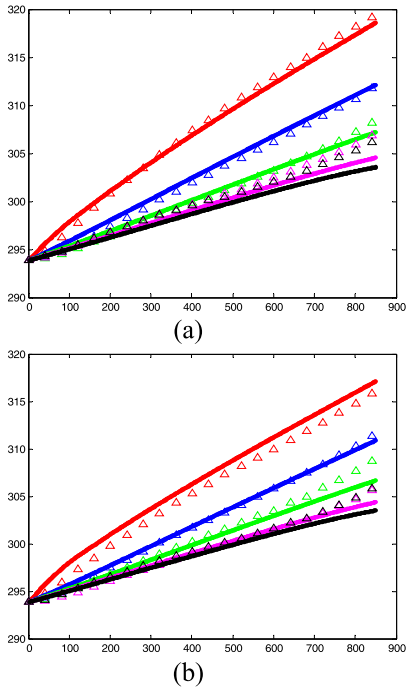

FIGURE 8. Temperature curve fitting of different thermocouples: (a) the first column (#1-#5); (b) the third column (#11-#15). Δ is–the measured temperature by the thermocouples and — is the predicted temperature.

respectively. The electrolyte material is mainly $LiPF_6$. The battery is first charged to the cut-off voltage of 3.65 V (theoretical capacity SOC=100%) at a constant current of C/8 rate (C-rate is the measurement of the charge and discharge current with respect to its nominal capacity), and then is charged at a constant voltage 3.65 V until the current is down to 1/20C rate [48]. The constant current constant voltage (CC/CV) charging algorithm is applied to charge the lithium battery to the fully charged state because of its simplicity and easy implementation [49]–[50]. This is the battery's fully charged state. Then, the battery is discharged at a rate of 3C (180A) until the cut-off voltage. As shown in Figure 3(a), a thermal chamber is applied to provide a space-efficient arrangement for effective thermal management of the battery while it is charging or discharging. The environmental temperature can be set to a certain value in the range of $-20^{\circ}C \sim 100^{\circ}C$ and is set to $25^{\circ}C$ here in the experiment.

As shown in Figure 3(b), the battery is put in the thermal chamber and electrically connected by an alligator clip. A Hall effect sensor is applied to measure the current; the terminal voltage is measured by the small alligator clip connected to the voltage metre, while the temperature data are collected by T-type thermocouples per second. There are 20 thermocouples evenly attached to the battery surface, which are represented by the dots (4coloums × 5 rows) in Figure 3(c). #1∼#20 refer to the locations of thermocouples attached on the battery surface.

B. RESULTS AND VALIDATION

The discharge time is 780 s and a total of 780 × 20 data are collected from the battery's experimental platform. The measured surface temperatures at different times are shown in Figure 4.

The measured surface temperature is taken for spatial BFs learning and model identification. The KL decomposition is then applied to these temperature data. The number of spatial BFs is set to N, which can be determined by the truncation criterion of the K-L method. According to (15), N is 5. Thus, five spatial BFs are obtained as shown in Figure 5.

The original time variables can be obtained by (16) while the truncated is also shown in Figures 6(a)-(e for comparison. The identified thermal parameters with the proposed method are shown in Table 1.

A contour function creates the temperature distribution from the discretized experimental data in MATLAB. As shown in Figure 7, the overall temperature distributions obtained from the experiment and the model show a good match. It is obvious that the temperature near the current-collecting tab of the positive electrode is higher than that of the negative electrode, because the comparatively larger ohmic resistance of the active material on the positive electrode is higher than that on the negative electrode. There will be more heat generated near the tabs of the positive electrode than the negative electrode with a similar current flow according to Ohm's law.

TABLE 1. Thermal parameter value.

Parameter	Initial value	Identified value
$k \ \ (wm^{-1}K^{-1})$	2.5231×10^{1}	2.9131×10^{1}
$C_p \ \ (Jkg^{-1}K^{-1})$	7.2365×10^{2}	8.0995×10^{2}
$\rho \ \ (kgm^{-3})$	1.9637×10^{3}	1.2932×10^{3}

Figure 8 compares the temperatures predicted by the proposed method and the temperatures measured by the 10 thermocouples (as shown in Figure 3©, #1-#5, #11-#15) during the 3 C discharge experiment. It can also be seen that the temperature near the positive tab (#1 and #11) increases faster than in any other location.

V. CONCLUSION

In this paper, a KL-Galerkin online modeling approach has been developed for the thermal model of a LIB cell. The Karhunen–Loève decomposition method and Galerkin's method are combined to obtain a space/time separation-based analytical model, which greatly reduces the complexity of the PDEs-based thermal model. The LM algorithm is first used to cooperate with the K-L decomposition-based model to identify the physical parameters of LIBs. The experimental results demonstrate the effectiveness of this method in estimating the temperature distribution of LIBs. A promising future research direction is to optimize the sensor placement with the proposed method.

REFERENCES

[1] C. Park and A. K. Jaura, "Dynamic thermal model of Li-ion battery for predictive behavior in hybrid and fuel cell vehicles," Warrendale, PA, USA, SAE Int., Tech. Paper, 2003, p. 2003-01-2286.
[2] X. Lin, A. G. Stefanopoulou, H. E. Perez, J. B. Siegel, Y. Li, and R. D. Anderson, "Quadruple adaptive observer of the core temperature in cylindrical li-ion batteries and their health monitoring," in Proc. Amer. Control Conf. (ACC), Jun. 2012, pp. 578–583.
[3] A. Subramaniam, S. Kolluri, C. D. Parke, M. Pathak, S. Santhanagopalan, and V. R. Subramanian, "Properly lumped lithium-ion battery models: A tanks-in-series approach," *J. Electrochem. Soc.*, vol. 167, no. 1, Jan. 2020, Art. no. 013534.
[4] M. L. Wang and H. X. Li, "Real-time estimation of temperature distribution for cylindrical lithium-ion batteries under boundary cooling," *IEEE Trans. Ind. Electron*, vol. 64, no. 3, pp. 966–977, Mar. 2017.
[5] Z. Liu and H.-X. Li, "A spatiotemporal estimation method for temperature distribution in lithium-ion batteries," *IEEE Trans. Ind. Informat.*, vol. 10, no. 4, pp. 2300–2307, Nov. 2014.
[6] S. Panchal, I. Dincer, M. Agelin-Chaab, R. Fraser, and M. Fowler, "Thermal modeling and validation of temperature distributions in a prismatic lithium-ion battery at different discharge rates and varying boundary conditions," *Appl. Thermal Eng.*, vol. 96, pp. 190–199, Mar. 2016.
[7] X. Lin, H. E. Perez, S. Mohan, J. B. Siegel, A. G. Stefanopoulou, Y. Ding, and M. P. Castanier, "A lumped-parameter electro-thermal model for cylindrical batteries," *J. Power Sources*, vol. 257, pp. 1–11, Jul. 2014.
[8] K. S. Hariharan, "A coupled nonlinear equivalent circuit—Thermal model for lithium ion cells," *J. Power Sources*, vol. 227, pp. 171–176, Apr. 2013.
[9] T. Yamanaka, D. Kihara, Y. Takagishi, and T. Yamaue, "Multi-physics equivalent circuit models for a cooling system of a lithium ion battery pack," *Batteries*, vol. 6, no. 3, p. 44, Aug. 2020.
[10] S. Panchal, I. Dincer, M. Agelin-Chaab, R. Fraser, and M. Fowler, "Experimental and theoretical investigation of temperature distributions in a prismatic lithium-ion battery," *Int. J. Thermal Sci.*, vol. 99, pp. 204–212, Jan. 2016.
[11] S. Panchal, I. Dincer, M. Agelin-Chaab, R. Fraser, and M. Fowler, "Experimental and theoretical investigations of heat generation rates for a water cooled $LiFePO_4$ battery," *Int. J. Heat Mass Transf.*, vol. 101, pp. 1093–1102, Oct. 2016.
[12] V. Ramadesigan, P. W. C. Northrop, S. De, S. Santhanagopalan, R. D. Braatz, and V. R. Subramanian, "Modeling and simulation of lithium-ion batteries from a systems engineering perspective," *J. Electrochem. Soc.*, vol. 159, no. 3, pp. R31–R45, Jan. 2012.
[13] W. B. Gu and C. Y. Wang, "Thermal-electrochemical modeling of battery systems," *J. Electrochem. Soc.*, vol. 147, no. 8, pp. 2910–2922, May 2000.
[14] K. Kumaresan, G. Sikha, and R. E. White, "Thermal model for a li-ion cell," *J. Electrochem. Soc.*, vol. 155, no. 2, p. A164, 2008.
[15] U. S. Kim, C. B. Shin, and C.-S. Kim, "Modeling for the scale-up of a lithium-ion polymer battery," *J. Power Sources*, vol. 189, no. 1, pp. 841–846, Apr. 2009.
[16] R. E. Gerver and J. P. Meyers, "Three-dimensional modeling of electrochemical performance and heat generation of lithium-ion batteries in tabbed planar configurations," *J. Electrochem. Soc.*, vol. 158, no. 7, p. A835, 2011.
[17] L. Guo and S. A. Billings, "State-space reconstruction and spatio-temporal prediction of lattice dynamical systems," *IEEE Trans. Autom. Control*, vol. 52, no. 4, pp. 622–632, Apr. 2007.
[18] D. Coca and S. A. Billings, "Identification of finite dimensional models of infinite dimensional dynamical systems," *Automatica*, vol. 38, no. 11, pp. 1851–1865, Nov. 2002.
[19] S. C. Chen, C. C. Wan, and Y. Y. Wang, "Thermal analysis of lithium-ion batteries," *J. Power Sources*, vol. 140, no. 1, pp. 111–124, 2005.
[20] M. W. Verbrugge, "Three-dimensionai temperature and current distribution in a battery module," *AIChE J.*, vol. 41, no. 6, pp. 1550–1562, Jun. 1995.
[21] K.-K. Xu, H.-X. Li, and H.-D. Yang, "Dual least squares support vector machines based spatiotemporal modeling for nonlinear distributed thermal processes," *J. Process Control*, vol. 54, pp. 81–89, Jun. 2017.
[22] L.-Q. Chen, H.-X. Li, and H.-D. Yang, "Dimension embedded basis function for spatiotemporal modeling of distributed parameter system," *IEEE Trans. Ind. Informat.*, vol. 16, no. 9, pp. 5846–5854, Sep. 2020.
[23] V. R. Subramanian, V. Boovaragavan, and V. D. Diwakar, "Toward real-time simulation of physics based lithium-ion battery models," *Electrochem. Solid-State Lett.*, vol. 10, no. 11, p. A255, 2007.
[24] V. Senthil Kumar, "Reduced order model for a lithium ion cell with uniform reaction rate approximation," *J. Power Sources*, vol. 222, pp. 426–441, Jan. 2013.
[25] M. Guo, X. Jin, and R. E. White, "An adaptive reduced-order-modeling approach for simulating real-time performances of li-ion battery systems," *J. Electrochem. Soc.*, vol. 164, no. 14, pp. A3602–A3613, Nov. 2017.
[26] L. Cai and R. E. White, "An efficient electrochemical–thermal model for a lithium-ion cell by using the proper orthogonal decomposition method," *J. Electrochem. Soc.*, vol. 157, no. 11, p. A1188, 2010.
[27] G. Fan, X. Li, and M. Canova, "A reduced-order electrochemical model of li-ion batteries for control and estimation applications," *IEEE Trans. Veh. Technol.*, vol. 67, no. 1, pp. 76–91, Jan. 2018.
[28] J. Meng, D.-I. Stroe, M. Ricco, G. Luo, and R. Teodorescu, "A simplified model-based state-of-charge estimation approach for lithium-ion battery with dynamic linear model," *IEEE Trans. Ind. Electron.*, vol. 66, no. 10, pp. 7717–7727, Oct. 2019.
[29] B.-C. Wang, H.-X. Li, and H.-D. Yang, "Spatial correlation-based incremental learning for spatiotemporal modeling of battery thermal process," *IEEE Trans. Ind. Electron.*, vol. 67, no. 4, pp. 2885–2893, Apr. 2020.
[30] B.-C. Wang and H.-X. Li, "A sliding window based dynamic spatiotemporal modeling for distributed parameter systems with time-dependent boundary conditions," *IEEE Trans. Ind. Informat.*, vol. 15, no. 4, pp. 2044–2053, Apr. 2019.
[31] K.-K. Xu, H.-X. Li, and H.-D. Yang, "Local-properties-embedding-based nonlinear spatiotemporal modeling for lithium-ion battery thermal process," *IEEE Trans. Ind. Electron.*, vol. 65, no. 12, pp. 9767–9776, Dec. 2018.

[32] K.-K. Xu, H.-X. Li, and Z. Liu, "ISOMAP-based spatiotemporal modeling for lithium-ion battery thermal process," *IEEE Trans. Ind. Informat.*, vol. 14, no. 2, pp. 569–577, Feb. 2018.
[33] S. Santhanagopalan, Q. Zhang, K. Kumaresan, and R. E. White, "Parameter estimation and life modeling of lithium-ion cells," *J. Electrochem. Soc.*, vol. 155, no. 4, p. A345, 2008.
[34] J. C. Forman, S. J. Moura, J. L. Stein, and H. K. Fathy, "Genetic identification and Fisher identifiability analysis of the Doyle–Fuller–Newman model from experimental cycling of a LiFePO4 cell," *J. Power Sources*, vol. 210, pp. 263–275, Jul. 2012.
[35] M. A. Rahman, S. Anwar, and A. Izadian, "Electrochemical model parameter identification of a lithium-ion battery using particle swarm optimization method," *J. Power Sources*, vol. 307, pp. 86–97, Mar. 2016.
[36] M. Luzi, M. Paschero, A. Rizzi, and F. M. Frattale Mascioli, "A PSO algorithm for transient dynamic modeling of lithium cells through a nonlinear RC filter," in *Proc. IEEE Congr. Evol. Comput. (CEC)*, Vancouver, BC, Canada, Jul. 2016, pp. 279–286.
[37] W.-J. Shen and H.-X. Li, "A sensitivity-based group-wise parameter identification algorithm for the electric model of li-ion battery," *IEEE Access*, vol. 5, pp. 4377–4387, Mar. 2017.
[38] A. Chandra Shekar and S. Anwar, "Real-time state-of-charge estimation via particle swarm optimization on a lithium-ion electrochemical cell model," *Batteries*, vol. 5, no. 1, p. 4, Jan. 2019.
[39] M. Paschero, G. L. Storti, A. Rizzi, F. M. F. Mascioli, and G. Rizzoni, "A novel mechanical analogy-based battery model for SoC estimation using a multicell EKF," *IEEE Trans. Sustain. Energy*, vol. 7, no. 4, pp. 1695–1702, Oct. 2016.
[40] N. Jin, D. L. Danilov, P. M. J. Van den Hof, and M. C. F. Donkers, "Parameter estimation of an electrochemistry-based lithium-ion battery model using a two-step procedure and a parameter sensitivity analysis," *Int. J. Energy Res.*, vol. 42, no. 7, pp. 2417–2430, Jun. 2018.
[41] U. S. Kim, J. Yi, C. B. Shin, T. Han, and S. Park, "Modeling the thermal behaviors of a lithium-ion battery during constant-power discharge and charge operations," *J. Electrochem. Soc.*, vol. 160, no. 6, pp. A990–A995, 2013.
[42] J. Yi, U. S. Kim, C. B. Shin, T. Han, and S. Park, "Three-dimensional thermal modeling of a lithium-ion battery considering the combined effects of the electrical and thermal contact resistances between current collecting tab and lead wire," *J. Electrochem. Soc.*, vol. 160, no. 3, pp. A437–A443, 2013.
[43] V. Srinivasan and C. Y. Wang, "Analysis of electrochemical and thermal behaviour of li-ion cells," *J. Electrochem. Soc.*, vol. 150, no. 1, pp. A98–A106. 2003.
[44] W.-J. Shen and H.-X. Li, "Multi-scale parameter identification of lithium-ion battery electric models using a PSO-LM algorithm," *Energies*, vol. 10, no. 4, p. 432, Mar. 2017.
[45] U. S. Kim, C. B. Shin, and C.-S. Kim, "Effect of electrode configuration on the thermal behavior of a lithium-polymer battery," *J. Power Sources*, vol. 180, no. 2, pp. 909–916, Jun. 2008.
[46] Z. Liu and H.-X. Li, "Extreme learning machine based spatiotemporal modeling of lithium-ion battery thermal dynamics," *J. Power Sources*, vol. 277, pp. 228–238, Mar. 2015.
[47] A. Constantinides and N. Mostoufi, *Numerical Methods for Chemical Engineers With MATLAB Applications*, vol. 4. Upper Saddle River, NJ, USA: Prentice-Hall, 1999, ch. 7, sec. 7.7, pp. 493–494.
[48] Y. Gao, J. Jiang, C. Zhang, W. Zhang, Z. Ma, and Y. Jiang, "Lithium-ion battery aging mechanisms and life model under different charging stresses," *J. Power Sources*, vol. 356, pp. 103–114, Jul. 2017.
[49] W. X. Shen, T. T. Vo, and A. Kapoor, "Charging algorithms of lithium-ion batteries: An overview," in *Proc. IEEE Conf. Ind. Electron. Appl.*, Jul. 2012, pp. 1567–1572.
[50] X. Wu, C. Hu, J. Du, and J. Sun, "Multistage CC-CV charge method for li-ion battery," *Math. Problems Eng.*, vol. 2015, pp. 1–10, Sep. 2015.

WENJING SHEN (Member, IEEE) received the B.E. and M.E. degrees in mechatronics engineering from Central South University, Changsha, China, in 2006 and 2009, respectively, and the Ph.D. degree in systems engineering and engineering management from the City University of Hong Kong, in 2017.

She is currently an Assistant Professor with the Sino-German College of Intelligent Manufacturing, Shenzhen Technology University, Guangdong, China. Her current research interests include modeling of thermal distribution in industrial processes, data-based modeling, and optimization.

KANGKANG XU (Member, IEEE) received the B.E. and Ph.D. degrees in mechatronics engineering from Central South University, Changsha, China, in 2012 and 2017, respectively.

He is currently a Lecturer with the School of Electro-Mechanical Engineering, Guangdong University of Technology, Guangzhou, China. His research interests include distributed parameter systems and intelligent modeling.

LIMING DENG received the B.E. degree in mechanical engineering from Nanchang University, in 2011, and the M.E. degree from Shanghai Jiao Tong University, China, in 2014, and the Ph.D. degree in systems engineering and engineering management from the City University of Hong Kong, in 2018.

He is currently a Research Scientist with Ping An Technology at Shenzhen. His research interests include prognostics and health management, bioinformatics, and natural language processing.

SHUPENG ZHANG (Member, IEEE) received the B.S. and M.S. degrees in automotive engineering from Tsinghua University, Beijing, China, in 2006 and 2009, respectively, and the Ph.D. degree in mechanical engineering from Michigan State University, MI, USA, in 2014.

He is currently an Associate Professor with the College of Urban Transportation and Logistics, Shenzhen Technology University, Guangdong, China. Prior to joining the university, he was a Control System Engineer of vehicle control with Karma Automotive LLC, California, USA. His current research interests include modelling and control of internal combustion engines, hybrid vehicle powertrain control and optimization, advanced control theory and applications, and so on.